where the left-hand side represents the optical path $FPAB$. Geometrically, we have $R \cos \psi + d = F$ and $F = R_0 + h_0$. Eliminating d and R_0, we find the lens profile:

$$R = \frac{F\left(1 - \frac{1}{n}\right)}{1 - \frac{1}{n} \cos \psi} \qquad (21.12.4)$$

which is recognized to be the equation for an ellipse with eccentricity and focal length $e = 1/n$ and $F_1 = F$.

In the above discussion, we considered only the refracted rays through the dielectric and ignored the reflected waves. These can be minimized by appropriate antireflection coatings.

22

Antenna Arrays

22.1 Antenna Arrays

Arrays of antennas are used to direct radiated power towards a desired angular sector. The number, geometrical arrangement, and relative amplitudes and phases of the array elements depend on the angular pattern that must be achieved.

Once an array has been designed to focus towards a particular direction, it becomes a simple matter to *steer* it towards some other direction by changing the relative phases of the array elements—a process called *steering* or *scanning*.

Figure 22.1.1 shows some examples of one- and two-dimensional arrays consisting of identical linear antennas. A linear antenna element, say along the z-direction, has an omnidirectional pattern with respect to the azimuthal angle ϕ. By replicating the antenna element along the x- or y-directions, the azimuthal symmetry is broken. By proper choice of the array feed coefficients a_n, any desired gain pattern $g(\phi)$ can be synthesized.

If the antenna element is replicated along the z-direction, then the omnidirectionality with respect to ϕ is maintained. With enough array elements, any prescribed polar angle pattern $g(\theta)$ can be designed.

In this section we discuss array design methods and consider various design issues, such as the tradeoff between beamwidth and sidelobe level.

For uniformly-spaced arrays, the design methods are identical to the methods for designing FIR digital filters in DSP, such as window-based and frequency-sampling designs. In fact, historically, these methods were first developed in antenna theory and only later were adopted and further developed in DSP.

22.2 Translational Phase Shift

The most basic property of an array is that the relative displacements of the antenna elements with respect to each other introduce relative *phase shifts* in the radiation vectors, which can then add constructively in some directions or destructively in others. This is a direct consequence of the translational phase-shift property of Fourier transforms: a translation in space or time becomes a phase shift in the Fourier domain.
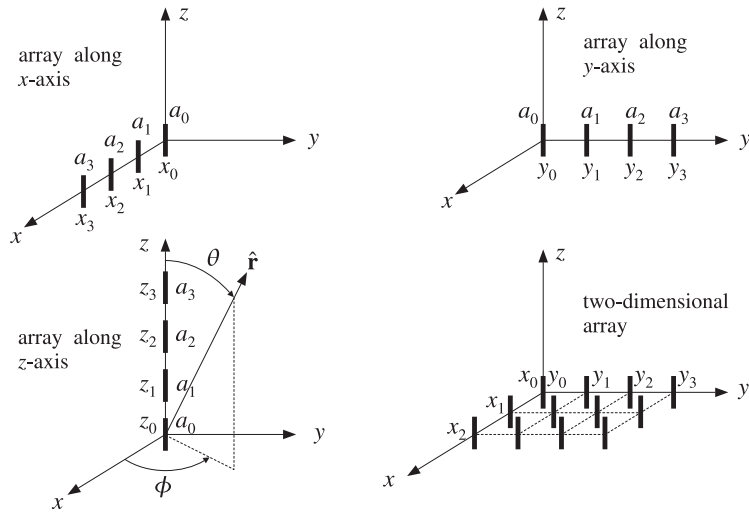
Fig. 22.1.1 Typical array configurations.

Figure 22.2.1 shows on the left an antenna translated by the vector $\mathbf{d}$, and on the right, several antennas translated to different locations and fed with different relative amplitudes.
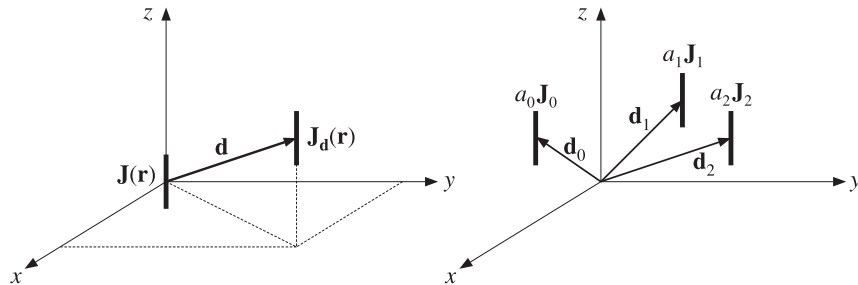

Fig. 22.2.1 Translated antennas.

The current density of the translated antenna will be $J_{\mathbf{d}}(\mathbf{r}) = J(\mathbf{r} - \mathbf{d})$. By definition, the radiation vector is the three-dimensional Fourier transform of the current density, as in Eq. (15.7.5). Thus, the radiation vector of the translated current will be:

$$F_{\mathbf{d}} = \int e^{j\mathbf{k}\cdot\mathbf{r}} J_{\mathbf{d}}(\mathbf{r}) \, d^3\mathbf{r} = \int e^{j\mathbf{k}\cdot\mathbf{r}} J(\mathbf{r} - \mathbf{d}) \, d^3\mathbf{r} = \int e^{j\mathbf{k}\cdot(\mathbf{r}'+\mathbf{d})} J(\mathbf{r}') \, d^3\mathbf{r}'$$

$$= e^{j\mathbf{k}\cdot\mathbf{d}} \int e^{j\mathbf{k}\cdot\mathbf{r}'} J(\mathbf{r}') \, d^3\mathbf{r}' = e^{j\mathbf{k}\cdot\mathbf{d}} F$$

where we changed variables to $\mathbf{r}' = \mathbf{r} - \mathbf{d}$. Thus,

$$\boxed{F_{\mathbf{d}}(\mathbf{k}) = e^{j\mathbf{k}\cdot\mathbf{d}} \, F(\mathbf{k})} \qquad \text{(translational phase shift)} \qquad (22.2.1)$$

22.3 Array Pattern Multiplication

More generally, we consider a three-dimensional array of several identical antennas located at positions $\mathbf{d}_0, \mathbf{d}_1, \mathbf{d}_2, \ldots$ with relative feed coefficients $a_0, a_1, a_2, \ldots$, as shown in Fig. 22.2.1. (Without loss of generality, we may set $\mathbf{d}_0 = 0$ and $a_0 = 1$.)

The current density of the nth antenna will be $J_n(\mathbf{r}) = a_n J(\mathbf{r} - \mathbf{d}_n)$ and the corresponding radiation vector:

$$F_n(\mathbf{k}) = a_n e^{j\mathbf{k}\cdot\mathbf{d}_n} \, F(\mathbf{k})$$

The total current density of the array will be:

$$J_{\text{tot}}(\mathbf{r}) = a_0 J(\mathbf{r} - \mathbf{d}_0) + a_1 J(\mathbf{r} - \mathbf{d}_1) + a_2 J(\mathbf{r} - \mathbf{d}_2) + \cdots$$

and the total radiation vector:

$$F_{\text{tot}}(\mathbf{k}) = F_0 + F_1 + F_2 + \cdots = a_0 e^{j\mathbf{k}\cdot\mathbf{d}_0} F(\mathbf{k}) + a_1 e^{j\mathbf{k}\cdot\mathbf{d}_1} F(\mathbf{k}) + a_2 e^{j\mathbf{k}\cdot\mathbf{d}_2} F(\mathbf{k}) + \cdots$$

The factor $F(\mathbf{k})$ due to a single antenna element at the origin is common to all terms. Thus, we obtain the *array pattern multiplication* property:

$$\boxed{F_{\text{tot}}(\mathbf{k}) = A(\mathbf{k}) F(\mathbf{k})} \qquad \text{(array pattern multiplication)} \qquad (22.3.1)$$

where $A(\mathbf{k})$ is the *array factor*:

$$\boxed{A(\mathbf{k}) = a_0 e^{j\mathbf{k}\cdot\mathbf{d}_0} + a_1 e^{j\mathbf{k}\cdot\mathbf{d}_1} + a_2 e^{j\mathbf{k}\cdot\mathbf{d}_2} + \cdots} \qquad \text{(array factor)} \qquad (22.3.2)$$

Since $\mathbf{k} = k\hat{\mathbf{r}}$, we may also denote the array factor as $A(\hat{\mathbf{r}})$ or $A(\theta, \phi)$. To summarize, the net effect of an array of identical antennas is to modify the single-antenna radiation vector by the array factor, which incorporates all the translational phase shifts and relative weighting coefficients of the array elements.

We may think of Eq. (22.3.1) as the input/output equation of a linear system with $A(\mathbf{k})$ as the *transfer function*. We note that the corresponding radiation intensities and power gains will also be related in a similar fashion:

$$\boxed{\begin{aligned} U_{\text{tot}}(\theta, \phi) &= |A(\theta, \phi)|^2 \, U(\theta, \phi) \\ G_{\text{tot}}(\theta, \phi) &= |A(\theta, \phi)|^2 \, G(\theta, \phi) \end{aligned}} \qquad (22.3.3)$$

where $U(\theta, \phi)$ and $G(\theta, \phi)$ are the radiation intensity and power gain of a single element. The array factor can dramatically alter the directivity properties of the single-antenna element. The power gain $|A(\theta, \phi)|^2$ of an array can be computed with the help of the MATLAB function `gain1d` of Appendix L with typical usage:

```
[g, phi] = gain1d(d, a, Nph);        % compute normalized gain of an array
```

Example 22.3.1: Consider an array of two isotropic antennas at positions $\mathbf{d}_0 = 0$ and $\mathbf{d}_1 = \hat{\mathbf{x}}d$
(alternatively, at $\mathbf{d}_0 = -(d/2)\hat{\mathbf{x}}$ and $\mathbf{d}_1 = (d/2)\hat{\mathbf{x}}$), as shown below:
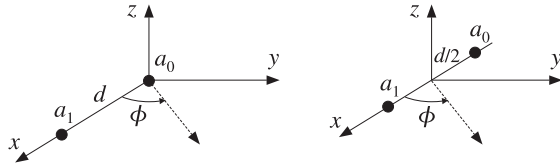
The displacement phase factors are:

$$e^{j\mathbf{k}\cdot\mathbf{d}_0} = 1\,, \qquad e^{j\mathbf{k}\cdot\mathbf{d}_1} = e^{jk_x d} = e^{jkd\sin\theta\cos\phi}$$

or, in the symmetric case:

$$e^{j\mathbf{k}\cdot\mathbf{d}_0} = e^{-jk_x d/2} = e^{-jk(d/2)\sin\theta\cos\phi}\,, \qquad e^{j\mathbf{k}\cdot\mathbf{d}_1} = e^{jk_x d/2} = e^{jk(d/2)\sin\theta\cos\phi}$$

Let $\mathbf{a} = [a_0, a_1]$ be the array coefficients. The array factor is:

$$A(\theta,\phi) = a_0 + a_1 e^{jkd\sin\theta\cos\phi}$$

$$A(\theta,\phi) = a_0 e^{-jk(d/2)\sin\theta\cos\phi} + a_1 e^{jk(d/2)\sin\theta\cos\phi}\,, \qquad \text{(symmetric case)}$$

The two expressions differ by a phase factor, which does not affect the power pattern. At
polar angle $\theta = 90^\circ$, that is, on the xy-plane, the array factor will be:

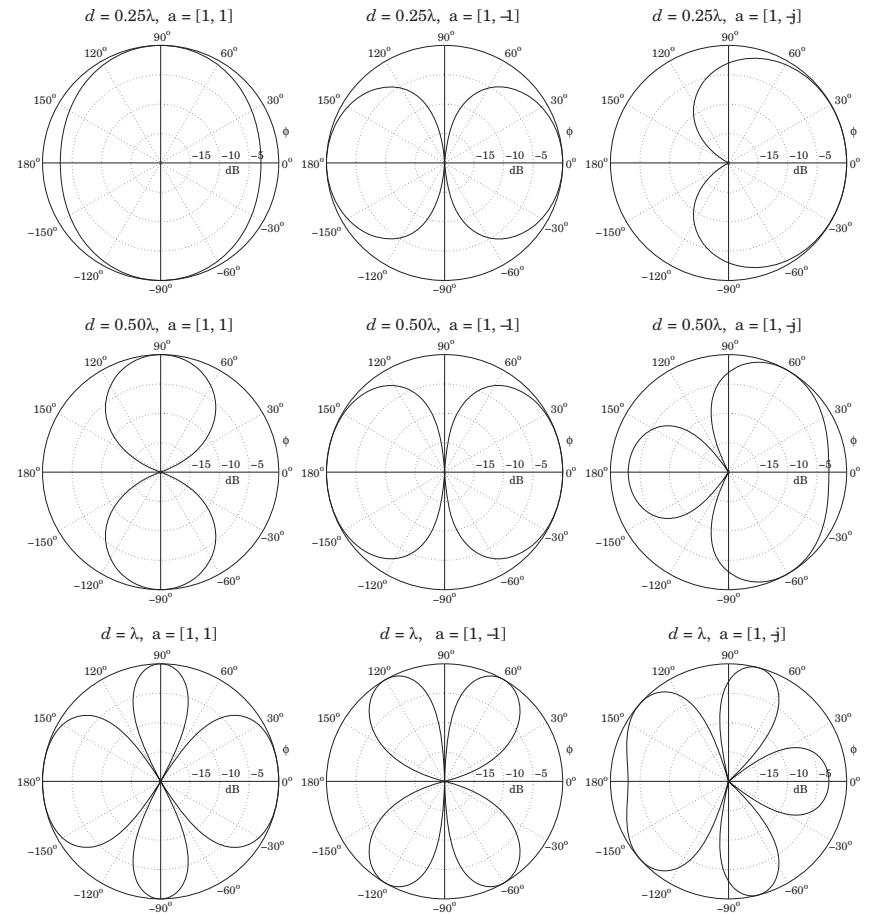$$A(\phi) = a_0 + a_1 e^{jkd\cos\phi}$$

and the azimuthal power pattern:

$$g(\phi) = |A(\phi)|^2 = |a_0 + a_1 e^{jkd\cos\phi}|^2$$

Note that $kd = 2\pi d/\lambda$. Figure 22.3.1 shows $g(\phi)$ for the array spacings $d = 0.25\lambda$,
$d = 0.50\lambda$, $d = \lambda$, or $kd = \pi/2, \pi, 2\pi$, and the following array weights:

$$\mathbf{a} = [a_0, a_1] = [1, 1]$$
$$\mathbf{a} = [a_0, a_1] = [1, -1] \qquad\qquad (22.3.4)$$
$$\mathbf{a} = [a_0, a_1] = [1, -j]$$

The first of these graphs was generated by the MATLAB code:

```
d = 0.25; a = [1,1];              % d is in units of λ
[g, phi] = gain1d(d, a, 400);     % 400 phi's in [0,π]
dbz(phi, g, 30, 20);              % 30° grid, 20-dB scale
```

Fig. 22.3.1 Azimuthal gain patterns of two-element isotropic array.

As the relative phase of a_0 and a_1 changes, the pattern rotates so that its main lobe is in
a different direction. When the coefficients are in phase, the pattern is broadside to the
array, that is, towards $\phi = 90^\circ$. When they are in anti-phase, the pattern is end-fire, that
is, towards $\phi = 0^\circ$ and $\phi = 180^\circ$.

The technique of rotating or steering the pattern towards some other direction by intro-
ducing relative phases among the elements is further discussed in Sec. 22.9. There, we
will be able to predict the steering angles of this example from the relative phases of the
weights.

Another observation from these graphs is that as the array pattern is steered from broad-
side to endfire, the widths of the main lobes become larger. We will discuss this effect in
Sects. 22.9 and 22.10.

When $d \geq \lambda$, more than one main lobes appear in the pattern. Such main lobes are called grating lobes or fringes and are further discussed in Sec. 22.6. Fig. 22.3.2 shows some additional examples of grating lobes for spacings $d = 2\lambda$, 4λ, and 8λ. □
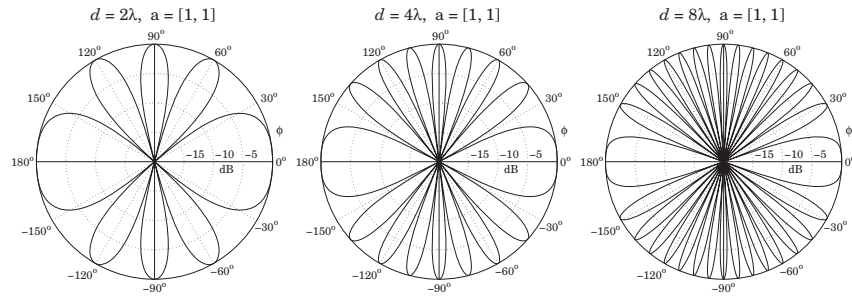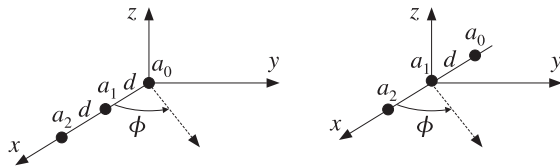

Fig. 22.3.2 Grating lobes of two-element isotropic array.

Example 22.3.2: Consider a three-element array of isotropic antennas at locations $\mathbf{d}_0 = 0$, $\mathbf{d}_1 = d\hat{\mathbf{x}}$, and $\mathbf{d}_2 = 2d\hat{\mathbf{x}}$, or, placed symmetrically at $\mathbf{d}_0 = -d\hat{\mathbf{x}}$, $\mathbf{d}_1 = 0$, and $\mathbf{d}_2 = d\hat{\mathbf{x}}$, as shown below:

The displacement phase factors evaluated at $\theta = 90^o$ are:

$$e^{j\mathbf{k}\cdot\mathbf{d}_0} = 1, \quad e^{j\mathbf{k}\cdot\mathbf{d}_1} = e^{jk_x d} = e^{jkd\cos\phi} \quad e^{j\mathbf{k}\cdot\mathbf{d}_2} = e^{j2k_x d} = e^{j2kd\cos\phi}$$

Let $\mathbf{a} = [a_0, a_1, a_2]$ be the array weights. The array factor is:

$$A(\phi) = a_0 + a_1 e^{jkd\cos\phi} + a_2 e^{2jkd\cos\phi}$$

Figure 22.3.3 shows $g(\phi) = |A(\phi)|^2$ for the array spacings $d = 0.25\lambda$, $d = 0.50\lambda$, $d = \lambda$, or $kd = \pi/2, \pi, 2\pi$, and the following choices for the weights:

$$\mathbf{a} = [a_0, a_1, a_2] = [1, 1, 1]$$

$$\mathbf{a} = [a_0, a_1, a_2] = [1, (-1), (-1)^2] = [1, -1, 1] \tag{22.3.5}$$

$$\mathbf{a} = [a_0, a_1, a_2] = [1, (-j), (-j)^2] = [1, -j, -1]$$

where in the last two cases, progressive phase factors of 180° and 90° have been introduced between the array elements.
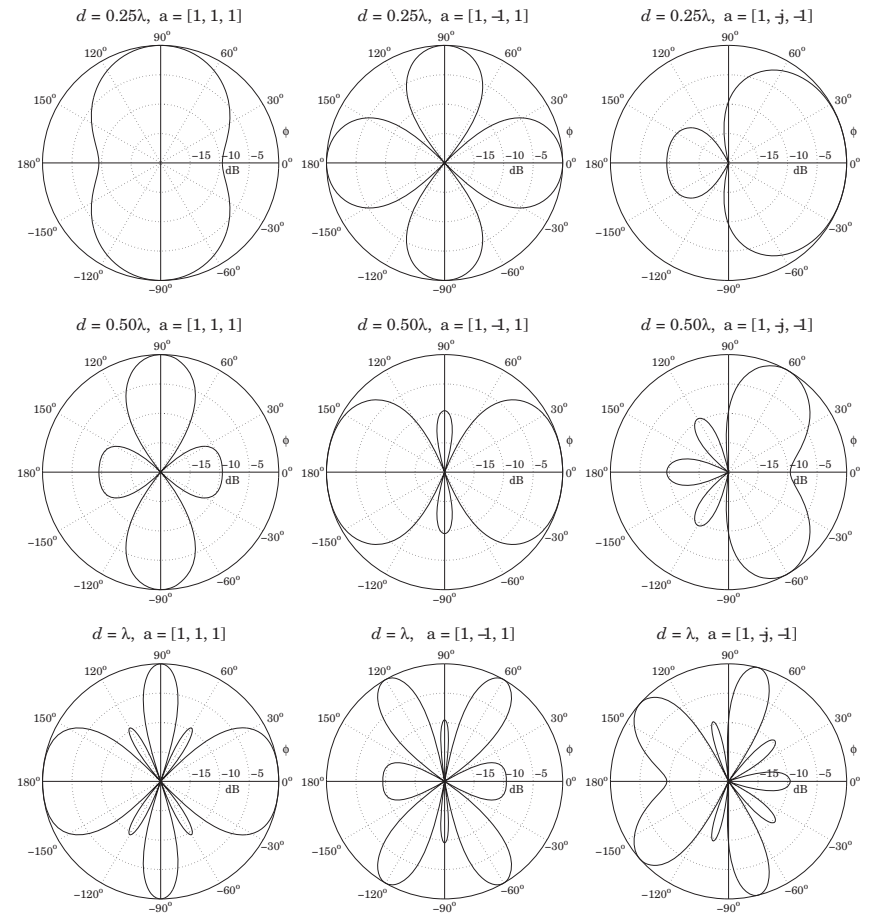
The MATLAB code for generating the last graph was:

Fig. 22.3.3 Azimuthal gains of three-element isotropic array.

```
d = 1; a = [1,-j,-1];
[g, phi] = gain1d(d, a, 400);
dbz(phi, g, 30, 20);
```

The patterns are similarly rotated as in the previous example. The main lobes are narrower, but we note the appearance of sidelobes at the level of -10 dB. We will see later that as the number of array elements increases, the sidelobes reach a constant level of about -13 dB for an array with uniform weights.

Such sidelobes can be reduced further if we use appropriate non-uniform weights, but at the expense of increasing the beamwidth of the main lobes. □

Example 22.3.3: As an example of a two-dimensional array, consider three z-directed half-wave dipoles: one at the origin, one on the x-axis, and one on the y-axis, both at a distance $d = \lambda/2$, as shown below.
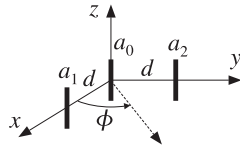
The relative weights are a_0, a_1, a_2. The displacement vectors are $\mathbf{d}_1 = \hat{\mathbf{x}}d$ and $\mathbf{d}_2 = \hat{\mathbf{y}}d$. Using Eq. (17.1.4), we find the translational phase-shift factors:

$$e^{j\mathbf{k}\cdot\mathbf{d}_1} = e^{jk_x d} = e^{jkd\sin\theta\cos\phi} , \qquad e^{j\mathbf{k}\cdot\mathbf{d}_2} = e^{jk_y d} = e^{jkd\sin\theta\sin\phi}$$

and the array factor:

$$A(\theta,\phi) = a_0 + a_1 e^{jkd\sin\theta\cos\phi} + a_2 e^{jkd\sin\theta\sin\phi}$$

Thus, the array's total normalized gain will be up to an overall constant:

$$g_{\text{tot}}(\theta,\phi) = |A(\theta,\phi)|^2 g(\theta,\phi) = |A(\theta,\phi)|^2 \left| \frac{\cos(0.5\pi\cos\theta)}{\sin\theta} \right|^2$$

The gain pattern on the xy-plane ($\theta = 90^\circ$) becomes:

$$g_{\text{tot}}(\phi) = \left| a_0 + a_1 e^{jkd\cos\phi} + a_2 e^{jkd\sin\phi} \right|^2$$

Note that because $d = \lambda/2$, we have $kd = \pi$. The omnidirectional case of a single element is obtained by setting $a_1 = a_2 = 0$ and $a_0 = 1$. Fig. 22.3.4 shows the gain $g_{\text{tot}}(\phi)$ for various choices of the array weights a_0, a_1, a_2.

Because of the presence of the a_2 term, which depends on $\sin\phi$, the gain is not necessarily symmetric for negative ϕ's. Thus, it must be evaluated over the entire azimuthal range $-\pi \leq \phi \leq \pi$. Then, it can be plotted with the help of the function dbz2 which assumes the gain is over the entire 2π range. For example, the last of these graphs was computed by:

```
d = 0.5; a0=1; a1=2; a2=2;
phi = (0:400) * 2*pi/400;
psi1 = 2*pi*d*cos(phi);
psi2 = 2*pi*d*sin(phi);
g = abs(a0 + a1 * exp(j*psi1) + a2 * exp(j*psi2)).^2;
g = g/max(g);
dbz2(phi, g, 45, 12);
```

When $a_2 = 0$, we have effectively a two-element array along the x-axis with equal weights. The resulting array pattern is broadside, that is, maximum along the perpendicular $\phi = 90^\circ$ to the array. Similarly, when $a_1 = 0$, the two-element array is along the y-axis and the pattern is broadside to it, that is, along $\phi = 0$. When $a_0 = 0$, the pattern is broadside to the line joining elements 1 and 2.   □
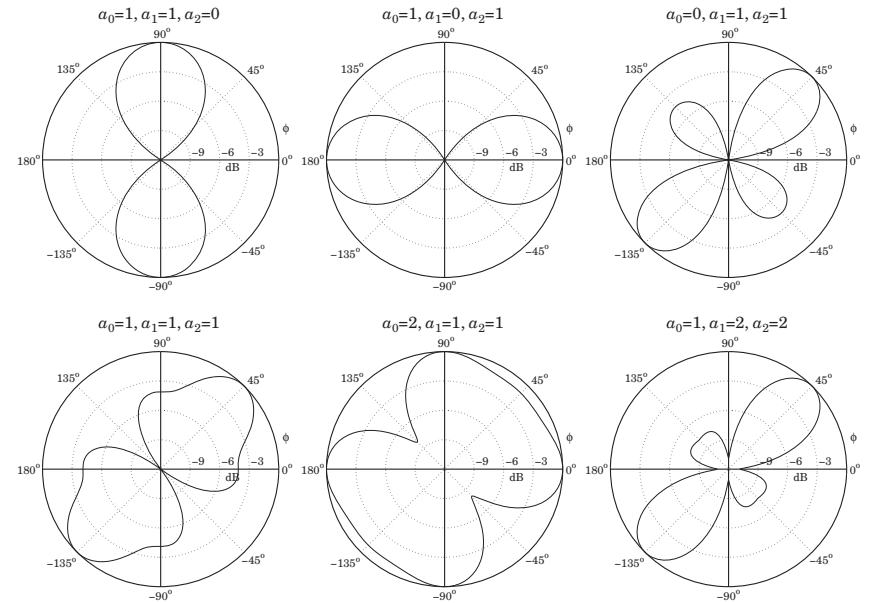
Fig. 22.3.4 Azimuthal gain patterns of two-dimensional array.

Example 22.3.4: The analysis of the rhombic antenna in Sec. 17.7 was carried out with the help of the translational phase-shift theorem of Eq. (22.2.1). The theorem was applied to antenna pairs 1, 3 and 2, 4.

A more general version of the translation theorem involves both a translation and a rotation (a Euclidean transformation) of the type $\mathbf{r}' = R^{-1}(\mathbf{r} - \mathbf{d})$, or, $\mathbf{r} = R\mathbf{r}' + \mathbf{d}$, where R is a rotation matrix.

The rotated/translated current density is then defined as $\mathbf{J}_{R,\mathbf{d}}(\mathbf{r}) = R^{-1}\mathbf{J}(\mathbf{r}')$ and the corresponding relationship between the two radiation vectors becomes:

$$\mathbf{F}_{R,\mathbf{d}}(\mathbf{k}) = e^{j\mathbf{k}\cdot\mathbf{d}} R^{-1} \mathbf{F}(R^{-1}\mathbf{k})$$

The rhombic as well as the vee antennas can be analyzed by applying such rotational and translational transformations to a single traveling-wave antenna along the z-direction, which is rotated by an angle $\pm\alpha$ and then translated.   □

Example 22.3.5: *Ground Effects Between Two Antennas.* There is a large literature on radio-wave propagation effects [19,34,44,1708–1724]. Consider a mobile radio channel in which the transmitting vertical antenna at the base station is at height h_1 from the ground and the receiving mobile antenna is at height h_2, as shown below. The ray reflected from the ground interferes with the direct ray and can cause substantial signal cancellation at the receiving antenna.
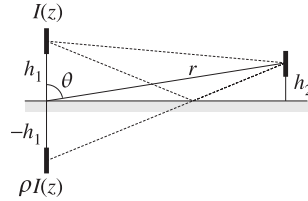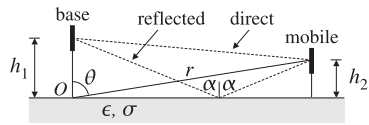
The reflected ray may be thought of as originating from the *image* of the transmitting antenna at $-h_1$, as shown. Thus, we have an equivalent two-element transmitting array. We assume that the currents on the actual and image antennas are $I(z)$ and $\rho I(z)$, where $\rho = -\rho_{TM}$ is the reflection coefficient of the ground for parallel polarization (the negative sign is justified in the next example), given in terms of the angle of incidence α by:

$$\rho = -\rho_{TM} = \frac{n^2 \cos\alpha - \sqrt{n^2 - \sin^2\alpha}}{n^2 \cos\alpha + \sqrt{n^2 - \sin^2\alpha}}, \qquad n^2 = \frac{\epsilon}{\epsilon_0} - j\frac{\sigma}{\omega\epsilon_0} = \epsilon_r - j\frac{\eta_0}{2\pi}\sigma\lambda$$

where n is the complex refractive index of the ground, and we replaced $\omega\epsilon_0 = 2\pi f\epsilon_0 = 2\pi c_0\epsilon_0/\lambda$ and $c_0\epsilon_0 = 1/\eta_0$. Numerically, we may set $\eta_0/2\pi \simeq 60\ \Omega$. From the geometry of the figure, we find that the angle α is related to the polar angle θ by:

$$\tan\alpha = \frac{r\sin\theta}{h_1 + r\cos\theta}$$

In the limit of large r, α tends to θ. For a perfectly conducting ground ($\sigma = \infty$), the reflection coefficient becomes $\rho = 1$, regardless of the incidence angle.

On the other hand, for an imperfect ground and for *low* grazing angles ($\alpha \simeq 90^\circ$), the reflection coefficient becomes $\rho = -1$, regardless of the conductivity of the ground. This is the relevant case in mobile communications.

The array factor can be obtained as follows. The two displaced antennas are at locations $\mathbf{d}_1 = h_1\hat{\mathbf{z}}$ and $\mathbf{d}_2 = -h_1\hat{\mathbf{z}}$, so that the displacement phase factors are:

$$e^{j\mathbf{k}\cdot\mathbf{d}_1} = e^{jk_z h_1} = e^{jkh_1\cos\theta}, \qquad e^{j\mathbf{k}\cdot\mathbf{d}_2} = e^{-jk_z h_1} = e^{-jkh_1\cos\theta}$$

where we replaced $k_z = k\cos\theta$. The relative feed coefficients are 1 and ρ. Therefore, the array factor and its magnitude will be:

$$A(\theta) = e^{jkh_1\cos\theta} + \rho e^{-jkh_1\cos\theta} = e^{jkh_1\cos\theta}(1 + \rho e^{-j\Delta})$$

$$|A(\theta)|^2 = |1 + \rho e^{-j\Delta}|^2, \quad \text{where} \quad \Delta = 2kh_1\cos\theta \tag{22.3.6}$$

The gain of the transmitting antenna becomes $G_{\text{tot}}(\theta) = |A(\theta)|^2 G(\theta)$, where $G(\theta)$ is the gain with the ground absent. For the common case of low grazing angles, or $\rho = -1$, the array factor becomes:

$$|A(\theta)|^2 = |1 - e^{-j\Delta}|^2 = 2 - 2\cos(\Delta) = 4\sin^2\left(\frac{\Delta}{2}\right)$$

At the location of the mobile antenna which is at height h_2, the geometry of the figure implies that $\cos\theta = h_2/r$. Thus, we have $\Delta = 2kh_1\cos\theta = 2kh_1h_2/r$, and

$$|A(\theta)|^2 = 4\sin^2\left(\frac{\Delta}{2}\right) \simeq \Delta^2 = \left(\frac{2kh_1h_2}{r}\right)^2$$

where we assumed that $kh_1h_2/r \ll 1$ and used the approximation $\sin x \simeq x$. Therefore, for fixed antenna heights h_1, h_2, the gain at the location of the receiving antenna drops like $1/r^2$. This is in addition to the $1/r^2$ drop arising from the power density. Thus, the presence of the ground reflection causes the overall power density at the receiving antenna to drop like $1/r^4$ instead of $1/r^2$.

For two antennas pointing towards the maximum gain of each other, the Friis transmission formula must be modified to read:

$$\frac{P_2}{P_1} = G_1 G_2 \left(\frac{\lambda}{4\pi r}\right)^2 |1 + \rho e^{-j\Delta}|^2, \qquad \Delta = \frac{2kh_1h_2}{r} = \frac{4\pi h_1 h_2}{\lambda r} \tag{22.3.7}$$

The direct and ground-reflected rays are referred to as the *space wave*. When both antennas are close to the ground, one must also include a term in $A(\theta)$ due to the so-called *Norton surface wave* [1719–1724]:

$$A(\theta) = \underbrace{1 + \rho e^{-j\Delta}}_{\text{space wave}} + \underbrace{(1 - \rho) F e^{-j\Delta}}_{\text{surface wave}}$$

where F is an attenuation coefficient that, for $kr \gg 1$, can be approximated by [1711]:

$$F = \frac{\sin^2\alpha}{jkr(\cos\alpha + u)^2}, \qquad u = \frac{1}{n^2}\sqrt{n^2 - \sin^2\alpha}$$

At grazing angles, the space-wave terms of $A(\theta)$ tend to cancel and the surface wave becomes the only means of propagation. A historical review of the ground-wave propagation problem and some of its controversies can be found in [1709]. $\quad\Box$

Example 22.3.6: *Vertical Dipole Antenna over Imperfect Ground.* Consider a vertical linear antenna at a height h over ground as shown below. When the observation point is far from the antenna, the direct and reflected rays r_1 and r_2 will be almost parallel to each other, forming an angle θ with the vertical. The incidence angle α of the previous example is then $\alpha = \theta$, so that the TM reflection coefficient is:

$$\rho_{TM} = \frac{\sqrt{n^2 - \sin^2\theta} - n^2\cos\theta}{\sqrt{n^2 - \sin^2\theta} + n^2\cos\theta}, \qquad n^2 = \epsilon_r - j\frac{\eta_0}{2\pi}\sigma\lambda$$
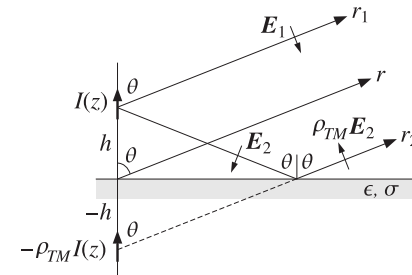
The relative permittivity $\epsilon_r = \epsilon/\epsilon_0$ and conductivity σ (in units of S/m) are given below for some typical grounds and typical frequencies:[†]

[†] ITU Recommendation ITU-R P.527-3 on the "Electrical Characteristics of the Surface of the Earth," 1992.

	1 MHz		100 MHz		1 GHz	
ground type	ϵ_r	σ	ϵ_r	σ	ϵ_r	σ
very dry ground	3	10^{-4}	3	10^{-4}	3	1.5×10^{-4}
medium dry ground	15	10^{-3}	15	1.5×10^{-3}	15	3.5×10^{-3}
wet ground	30	10^{-2}	30	1.5×10^{-2}	30	1.5×10^{-1}
fresh water	80	3×10^{-3}	80	5×10^{-3}	80	1.5×10^{-1}
sea water	70	5	70	5	70	5

According to Eq. (17.1.6), the electric fields E_1 and E_2 along the direct and reflected rays will point in the direction of their respective polar unit vector $\hat{\boldsymbol{\theta}}$, as seen in the above figure. According to the sign conventions of Sec. 7.2, the reflected field $\rho_{TM}E_2$ will be pointing in the $-\hat{\boldsymbol{\theta}}$ direction, opposing E_1. The net field at the observation point will be:

$$E = E_1 - \rho_{TM}E_2 = \hat{\boldsymbol{\theta}}\, jk\eta\, \frac{e^{-jkr_1}}{4\pi r_1}F_z(\theta)\sin\theta - \hat{\boldsymbol{\theta}}\, jk\eta\, \frac{e^{-jkr_2}}{4\pi r_2}\rho_{TM}F_z(\theta)\sin\theta$$

where $F(\theta)=\hat{z}\,F_z(\theta)$ is the assumed radiation vector of the linear antenna. Thus, the reflected ray appears to have originated from an image current $-\rho_{TM}I(z)$. Using the approximations $r_1 = r - h\cos\theta$ and $r_2 = r + h\cos\theta$ in the propagation phase factors e^{-jkr_1} and e^{-jkr_2}, we obtain for the net electric field at the observation point (r,θ):

$$E = \hat{\boldsymbol{\theta}}\, jk\eta\, \frac{e^{-jkr}}{4\pi r}F_z(\theta)\sin\theta\,[e^{jkh\cos\theta} - \rho_{TM}e^{-jkh\cos\theta}]$$

It follows that the (unnormalized) gain will be:

$$g(\theta) = \left| F_z(\theta)\sin\theta \right|^2 \left| 1 - \rho_{TM}(\theta)e^{-2jkh\cos\theta} \right|^2$$

The results of the previous example are obtained if we set $\rho = -\rho_{TM}$. For a Hertzian dipole, we may replace $F_z(\theta)$ by unity. For a half-wave dipole, we have:

$$g(\theta) = \left| \frac{\cos(0.5\pi\cos\theta)}{\sin\theta} \right|^2 \left| 1 - \rho_{TM}(\theta)e^{-2jkh\cos\theta} \right|^2$$

Fig. 22.3.5 shows the resulting gains for a half-wave dipole at heights $h = \lambda/4$ and $h = \lambda/2$ and at frequencies $f = 1$ MHz and $f = 100$ MHz. The ground parameters correspond to the *medium dry* case of the above table. The dashed curves represent the gain of a single dipole, that is, $G(\theta) = \left| \cos(0.5\pi\cos\theta)/\sin\theta \right|^2$.

The following MATLAB code illustrates the generation of these graphs:

```
sigma=1e-3; ep0=8.854e-12; er=15; f=1e6; h = 1/4;
n2 = er - j*sigma/ep0/2/pi/f;

th = linspace(0,pi/2,301); c =cos(th); s2 = sin(th).^2;
rho = (sqrt(n2-s2) - n2*c)./(sqrt(n2-s2) + n2*c);
A = 1 - rho .* exp(-j*4*pi*h*cos(th));      % array factor
G = cos(pi*cos(th)/2)./sin(th); G(1)=0;     % half-wave dipole gain

g = abs(G.*A).^2;  g = g/max(g);            % normalized gain

dbp(th, g, 30, 12);                         % polar plot in dB
```
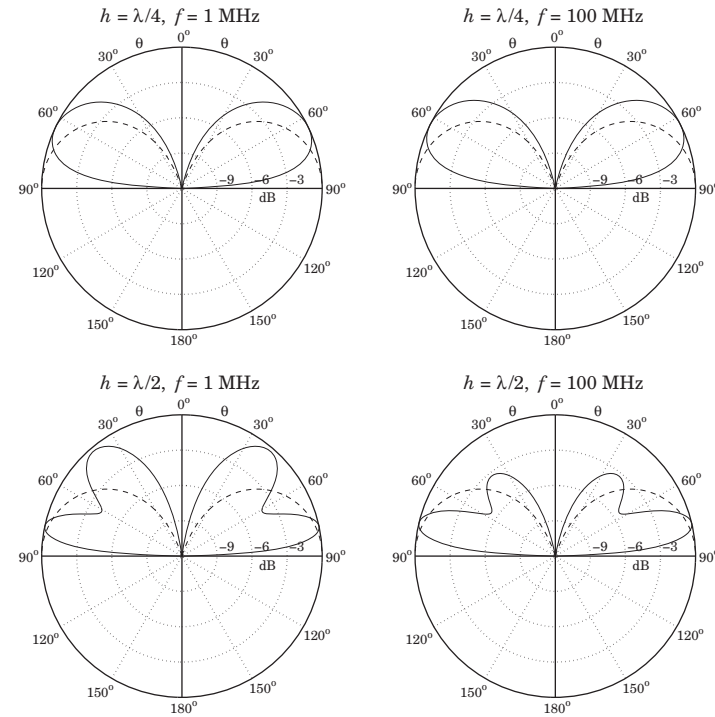

Fig. 22.3.5 Vertical dipole over imperfect ground

Thus, the presence of the ground significantly alters the angular gain of the dipole. For the case $h = \lambda/2$, we observe the presence of grating lobes, arising because the effective separation between the dipole and its image is $2h > \lambda/2$.

The number of grating lobes increases with the height h. These can be observed by running the above example code with $f = 1$ GHz (i.e., $\lambda = 30$ cm) for a cell phone held vertically at a height of $h = 6\lambda = 1.8$ meters. □

22.4 One-Dimensional Arrays

Next, we consider uniformly-spaced one-dimensional arrays. An array along the x-axis (see Fig. 22.3.4) with elements positioned at locations x_n, $n = 0, 1, 2, \ldots$, will have displacement vectors $\mathbf{d}_n = x_n\hat{x}$ and array factor:

$$A(\theta,\phi) = \sum_n a_n e^{j\mathbf{k}\cdot\mathbf{d}_n} = \sum_n a_n e^{jk_x x_n} = \sum_n a_n e^{jkx_n\sin\theta\cos\phi}$$

where we set $k_x = k\sin\theta\cos\phi$. For equally-spaced arrays, the element locations are $x_n = nd$, where d is the distance between elements. In this case, the array factor be-

comes:

$$A(\theta, \phi) = \sum_n a_n e^{jnkd \sin \theta \cos \phi} \qquad (22.4.1)$$

Because the angular dependence comes through the factor $k_x d = kd \sin \theta \cos \phi$, we are led to define the variable:

$$\psi = k_x d = kd \sin \theta \cos \phi \qquad \text{(digital wavenumber)} \qquad (22.4.2)$$

Then, the array factor may be thought of as a function of ψ:

$$A(\psi) = \sum_n a_n e^{j\psi n} \qquad \text{(array factor in digital wavenumber space)} \qquad (22.4.3)$$

The variable ψ is a normalized version of the wavenumber k_x and is measured in units of radians per (space) sample. It may be called a normalized *digital wavenumber*, in analogy with the time-domain normalized *digital frequency* $\omega = \Omega T = 2\pi f/f_s$, which is in units of radians per (time) sample.[†] The array factor $A(\psi)$ is the wavenumber version of the frequency response of a digital filter defined by

$$A(\omega) = \sum_n a_n e^{-j\omega n} \qquad (22.4.4)$$

We note the difference in the sign of the exponent in the definitions (22.4.3) and (22.4.4). This arises from the difference in defining time-domain and space-domain Fourier transforms, or from the difference in the sign for a plane wave, that is,

$$e^{j\omega t - j\mathbf{k} \cdot \mathbf{r}}$$

The wavenumber ψ is defined similarly for arrays along the y- or z-directions. In summary, we have the definitions:

$$\begin{aligned}
\psi &= k_x d = kd \sin \theta \cos \phi &\quad \text{(array along x-axis)}\\
\psi &= k_y d = kd \sin \theta \sin \phi &\quad \text{(array along y-axis)}\\
\psi &= k_z d = kd \cos \theta &\quad \text{(array along z-axis)}
\end{aligned} \qquad (22.4.5)$$

The array factors for the y- and z-axis arrays shown in Fig. 22.1.1 will be:

$$A(\theta, \phi) = \sum_n a_n e^{jk_y y_n} = \sum_n a_n e^{jk y_n \sin \theta \sin \phi}$$

$$A(\theta, \phi) = \sum_n a_n e^{jk_z z_n} = \sum_n a_n e^{jk z_n \cos \theta}$$

where $y_n = nd$ and $z_n = nd$. More generally, for an array along some arbitrary direction, we have $\psi = kd \cos \gamma$, where γ is the angle measured from the direction of the array.

[†]Here, Ω denotes the physical frequency in radians/sec.

The two most commonly used conventions are to assume either an array along the z-axis, or an array along the x-axis and measure its array factor only on the xy-plane, that is, at polar angle $\theta = 90°$. In these cases, we have:

$$\begin{aligned}
\psi &= k_x d = kd \cos \phi &\quad \text{(array along x-axis, with $\theta = 90°$)}\\
\psi &= k_z d = kd \cos \theta &\quad \text{(array along z-axis)}
\end{aligned} \qquad (22.4.6)$$

For the x-array, the azimuthal angle varies over $-\pi \le \phi \le \pi$, but the array response is symmetric in ϕ and can be evaluated only for $0 \le \phi \le \pi$. For the z-array, the polar angle varies over $0 \le \theta \le \pi$.

In analogy with time-domain DSP, we may also define the spatial analog of the z-plane by defining the variable $z = e^{j\psi}$ and the corresponding z-transform:

$$A(z) = \sum_n a_n z^n \qquad \text{(array factor in spatial z-domain)} \qquad (22.4.7)$$

The difference in sign between the space-domain and time-domain definitions is also evident here, where the expansion is in powers of z^n instead of z^{-n}. The array factor $A(\psi)$ may be called the *discrete-space Fourier transform* (DSFT) of the array weighting sequence a_n, just like the discrete-time Fourier transform (DTFT) of the time-domain case. The corresponding inverse DSFT is obtained by

$$a_n = \frac{1}{2\pi} \int_{-\pi}^{\pi} A(\psi) e^{-j\psi n} d\psi \qquad \text{(inverse DSFT)} \qquad (22.4.8)$$

This inverse transform forms the basis of most design methods for the array coefficients. As we mentioned earlier, such methods are identical to the methods of designing FIR filters in DSP. Various correspondences between the fields of array processing and time-domain digital signal processing are shown in Table 22.4.1.

Example 22.4.1: The array factors and z-transforms for Example 22.3.1 are for the three choices for the coefficients:

$$\begin{aligned}
A(\psi) &= 1 + e^{j\psi}, &\quad A(z) &= 1 + z\\
A(\psi) &= 1 - e^{j\psi}, &\quad A(z) &= 1 - z\\
A(\psi) &= 1 - j e^{j\psi}, &\quad A(z) &= 1 - jz
\end{aligned}$$

where $z = e^{j\psi}$ and $\psi = kd \cos \phi$. □

22.5 Visible Region

Because the correspondence from the physical angle-domain to the wavenumber ψ-domain is through the mapping (22.4.5) or (22.4.6), there are some additional subtleties that arise in the array processing case that do not arise in time-domain DSP. We note first that the array factor $A(\psi)$ is periodic in ψ with period 2π, and therefore, it is enough to know it within one Nyquist interval, that is, $-\pi \le \psi \le \pi$.

discrete-time signal processing	discrete-space array processing
time-domain sampling $t_n = nT$	space-domain sampling $x_n = nd$
sampling time interval T	sampling space interval d
sampling rate $1/T$ [samples/sec]	sampling rate $1/d$ [samples/meter]
frequency Ω	wavenumber k_x
digital frequency $\omega = \Omega T$	digital wavenumber $\psi = k_x d$
Nyquist interval $-\pi \le \omega \le \pi$	Nyquist interval $-\pi \le \psi \le \pi$
sampling theorem $\Omega \le \pi/T$	sampling theorem $k_x \le \pi/d$
spectral images	grating lobes or fringes
frequency response $A(\omega)$	array factor $A(\psi)$
z-domain $z = e^{j\omega}$	z-domain $z = e^{j\psi}$
transfer function $A(z)$	transfer function $A(z)$
DTFT and inverse DTFT	DSFT and inverse DSFT
pure sinusoid $e^{j\omega_0 n}$	narrow beam $e^{-j\psi_0 n}$
windowed sinusoid $w(n)e^{j\omega_0 n}$	windowed narrow beam $w(n)e^{-j\psi_0 n}$
resolution of multiple sinusoids	resolution of multiple beams
frequency shifting by AM modulation	phased array scanning
filter design by window method	array design by window method
bandpass FIR filter design	angular sector array design
frequency-sampling design	Woodward-Lawson design
DFT	Blass matrix
FFT	Butler matrix

Table 22.4.1 Duality between time-domain and space-domain signal processing.

However, the actual range of variation of ψ depends on the value of the quantity $kd = 2\pi d/\lambda$. As the azimuthal angle ϕ varies from 0° to 180°, the quantity $\psi = kd\cos\phi$, defined in Eq. (22.4.6), varies from $\psi = kd$ to $\psi = -kd$. Thus, the overall range of variation of ψ—called the *visible region*—will be:

$$-kd \le \psi \le kd \qquad \text{(visible region)} \qquad (22.5.1)$$

The total width of this region is $\psi_{\text{vis}} = 2kd$. Depending on the value of kd, the visible region can be less, equal, or more than one Nyquist interval:

$$
\begin{aligned}
d < \lambda/2 &\Rightarrow kd < \pi &\Rightarrow &\psi_{\text{vis}} < 2\pi &\text{(less than Nyquist)} \\
d = \lambda/2 &\Rightarrow kd = \pi &\Rightarrow &\psi_{\text{vis}} = 2\pi &\text{(full Nyquist)} \\
d > \lambda/2 &\Rightarrow kd > \pi &\Rightarrow &\psi_{\text{vis}} > 2\pi &\text{(more than Nyquist)}
\end{aligned}
\qquad (22.5.2)
$$

The visible region can also be viewed as that part of the unit circle covered by the angle range (22.5.1), as shown in Fig. 22.5.1. If $kd < \pi$, the visible region is the arc $z_a z z_b$ with the point $z = e^{j\psi}$ moving *clockwise* from z_a to z_b as ϕ varies from 0 to π. In the case $kd = \pi$, the starting and ending points, z_a and z_b, coincide with the $\psi = \pi$ point on the circle and the visible region becomes the entire circle. If $kd > \pi$, the visible region is one complete circle starting and ending at z_a and then continuing on to z_b.
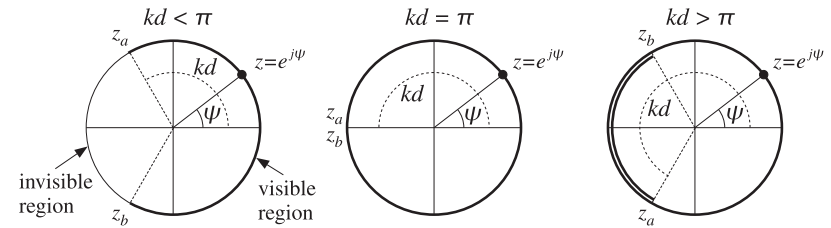
Fig. 22.5.1 Visible regions on the unit circle.

In all cases, the inverse transform (22.4.8) requires that we know $A(\psi)$ over one complete Nyquist interval. Therefore, in the case $kd < \pi$, we must specify appropriate values of the array factor $A(\psi)$ over the invisible region.

22.6 Grating Lobes

In the case $kd > \pi$, the values of $A(\psi)$ are over-specified and repeat over the visible region. This can give rise to *grating lobes* or *fringes*, which are mainbeam lobes in directions other than the desired one. We saw some examples in Figs. 22.3.1 and 22.3.2.

Grating lobes are essentially the *spectral images* generated by the sampling process (in this case, sampling in space.) In ψ-space, these images fall in Nyquist intervals other than the central one.

The number of grating lobes in an array pattern is the number of complete Nyquist intervals fitting within the width of the visible region, that is, $m = \psi_{\text{vis}}/2\pi = kd/\pi = 2d/\lambda$. For example in Fig. 22.3.2, the number of grating lobes are $m = 4, 8, 16$ for $d = 2\lambda, 4\lambda, 8\lambda$ (the two endfire lobes count as one.)

In most array applications grating lobes are undesirable and can be avoided by requiring that $kd < 2\pi$, or $d < \lambda$. It should be noted, however, that this condition does not necessarily avoid aliasing—it only avoids grating lobes. Indeed, if d is in the range $\lambda/2 < d < \lambda$, or, $\pi < kd < 2\pi$, part of the Nyquist interval repeats as shown in Fig. 22.5.1. To completely avoid repetitions, we must have $d \le \lambda/2$, which is equivalent to the *sampling theorem* condition $1/d \ge 2/\lambda$.

Grating lobes are desirable and useful in interferometry applications, such as *radio interferometry* used in radio astronomy. A simple interferometer is shown in Fig. 22.6.1. It consists of an array of two antennas separated by $d \gg \lambda$, so that hundreds or even thousands of grating lobes appear.

These lobes are extremely narrow allowing very small angular resolution of radio sources in the sky. The receiver is either an adder or a cross-correlator of the two antenna outputs. For an adder and identical antennas with equal weights, the output will be proportional to the array gain:

$$g(\phi) = \left| 1 + e^{jkd\cos\phi} \right|^2 = 2 + 2\cos(kd\cos\phi)$$

For a cross-correlator, the output will be proportional to $\cos(\Omega\tau)$, where τ is the time delay between the received signals. This delay is the time it takes the wavefront to
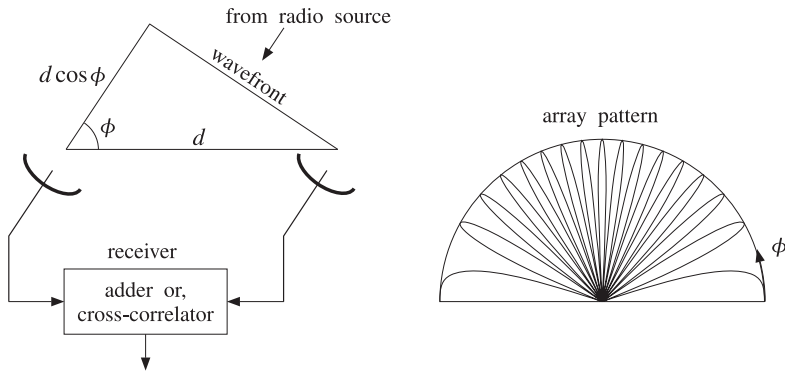
Fig. 22.6.1 Two-element interferometer and typical angular pattern.

travel the distance $d\cos\phi$, as shown in Fig. 22.6.1, that is, $\tau = (d\cos\phi)/c$. Therefore,

$$\cos(\Omega\tau) = \cos\left(\frac{2\pi f d\cos\phi}{c}\right) = \cos(kd\cos\phi)$$

In either case, the output is essentially $\cos(kd\cos\phi)$, and thus, exhibits the grating-lobe behavior. Cross-correlating interferometers are more widely used because they are more broadband.

The Very Large Array (VLA) radio telescope in New Mexico consists of 27 dish antennas with 25-m diameters. The antennas are on rails extending in three different directions to distances of up to 21 km. For each configuration, the number of possible interferometer pairs of antennas is $27(27-1)/2 = 351$. These 351 outputs can be used to make a "radio" picture of the source. The achievable resolution is comparable to that of optical telescopes (about 1 arc second.)

The Very Long Baseline Array (VLBA) consists of ten 25-m antennas located throughout the continental US, Puerto Rico, and Hawaii. The antennas are not physically connected to each other. Rather, the received signals at each antenna are digitally recorded, with the antennas being synchronized with atomic frequency standards, and then the recorded signals are digitally cross-correlated and processed off-line. The achievable resolution is about one milli-arc-second.

We note finally that in an interferometer, the angular pattern of each antenna element must also be taken into account because it multiplies the array pattern.

Example 22.6.1: In Fig. 22.3.2, we assumed isotropic antennas. Here, we look at the effect of the element patterns. Consider an array of two identical z-directed half-wavelength dipole antennas positioned along the z-axis at locations $z_0 = 0$ and $z_1 = d$. The total polar gain pattern will be the product of the array gain factor and the gain of each dipole:

$$g_{\text{tot}}(\theta) = |A(\theta)|^2 g_{\text{dipole}}(\theta) = \left|a_0 + a_1 e^{jkd\cos\theta}\right|^2 \left|\frac{\cos(0.5\pi\cos\theta)}{\sin\theta}\right|^2$$

Fig. 22.6.2 shows the effect of the element pattern for the case $d = 8\lambda$ and uniform weights $\mathbf{a} = [a_0, a_1] = [1, 1]$. The figure on the left represents the array factor, with the element pattern superimposed (dashed gain). On the right is the total gain.
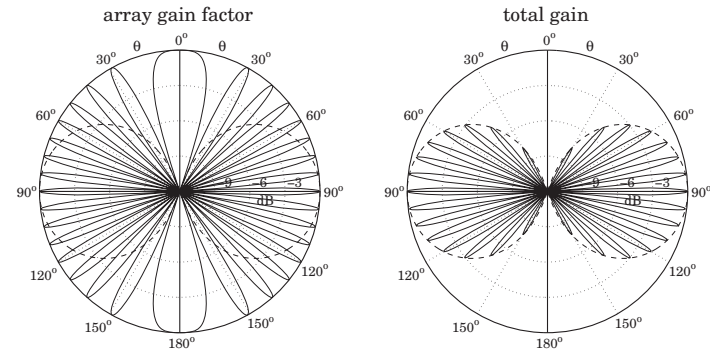
Fig. 22.6.2 Grating lobes of two half-wavelength dipoles separated by $d = 8\lambda$.

The MATLAB code used to generate the right graph was as follows:

```
d=8; a=[1,1];
[g, th] = gain1d(d, a, 400);
gdip = dipole(0.5, 400);
gtot = g .* gdip;
dbp(th, gtot, 30, 12);
dbadd(1, '--', th, gdip, 30, 12);                                  □
```

22.7 Uniform Arrays

The simplest one-dimensional array is the uniform array having equal weights. For an array of N isotropic elements at locations $x_n = nd$, $n = 0, 1, \ldots, N-1$, we define:

$$\mathbf{a} = [a_0, a_1, \ldots, a_{N-1}] = \frac{1}{N}[1, 1, \ldots, 1] \tag{22.7.1}$$

so that the sum of the weights is unity. The corresponding array polynomial and array factor are:

$$A(z) = \frac{1}{N}\left[1 + z + z^2 + \cdots + z^{N-1}\right] = \frac{1}{N}\frac{z^N - 1}{z - 1}$$

$$A(\psi) = \frac{1}{N}\left[1 + e^{j\psi} + e^{2j\psi} + \cdots + e^{(N-1)j\psi}\right] = \frac{1}{N}\frac{e^{jN\psi} - 1}{e^{j\psi} - 1} \tag{22.7.2}$$

where $z = e^{j\psi}$ and $\psi = kd\cos\phi$ for an array along the x-axis and look direction on the xy-plane. We may also write $A(\psi)$ in the form:

$$\boxed{A(\psi) = \frac{\sin\left(\frac{N\psi}{2}\right)}{N\sin\left(\frac{\psi}{2}\right)} e^{j(N-1)\psi/2}} \quad \text{(uniform array)} \tag{22.7.3}$$

The array factor (22.7.2) is the spatial analog of a lowpass FIR averaging filter in discrete-time DSP. It may also be viewed as a window-based narrow-beam design using a *rectangular* window. From this point of view, Eq. (22.7.3) is the DSFT of the rectangular window.

The array factor has been normalized to have unity gain at dc, that is, at zero wavenumber $\psi = 0$, or at the broadside azimuthal angle $\phi = 90^o$. The normalized power gain of the array will be:

$$g(\phi) = |A(\psi)|^2 = \left| \frac{\sin(N\psi/2)}{N\sin(\psi/2)} \right|^2 = \left| \frac{\sin((Nkd/2)\cos\phi)}{N\sin((kd/2)\cos\phi)} \right|^2 \qquad (22.7.4)$$

Although (22.7.2) defines the array factor for all ψ over one Nyquist interval, the actual visible region depends on the value of kd.

Fig. 22.7.1 shows $A(\psi)$ evaluated only over its visible region for an 8-element ($N = 8$) array, for the following three choices of the element spacing: $d = 0.25\lambda$, $d = 0.5\lambda$, and $d = \lambda$. The following MATLAB code generates the last two graphs:

```
d=1; N=8;
a = uniform(d, 90, N);
[g, phi] = gain1d(d, a, 400);
A = sqrt(g);
psi = 2*pi*d*cos(phi);
plot(psi/pi, A);
figure(2);
dbz(phi, g, 45, 20);
```

As ϕ varies from 0° to 180°, the visible regions for the three cases are:

$$
\begin{aligned}
d &= 0.25\lambda, & \psi &= (\pi/2)\cos\phi & \Rightarrow & & -\pi/2 &\le \psi \le \pi/2 \\
d &= 0.5\lambda, & \psi &= \pi\cos\phi & \Rightarrow & & -\pi &\le \psi \le \pi \\
d &= \lambda, & \psi &= 2\pi\cos\phi & \Rightarrow & & -2\pi &\le \psi \le 2\pi
\end{aligned}
$$

Thus, in the first case the visible region is only half of the Nyquist interval; in the second case, it is the full interval; and in the third case, the Nyquist interval is covered twice, and therefore, grating lobes will appear. Because $\psi = 2\pi\cos\phi$, the grating lobes at $\psi = \pm 2\pi$ correspond to the endfire angles of $\phi = 0^o$ and 180° (the larger width of the endfire lobes is explained in Sec. 22.10.)

The $N - 1$ zeros of the array polynomial $A(z)$ are the N-th roots of unity, except for the root at $z = 1$, that is,

$$z_i = e^{j\psi_i}, \quad \psi_i = \frac{2\pi i}{N}, \quad i = 1, 2, \ldots, N-1$$

Because these zeros lie on the unit circle, they will correspond to nulls in the angular pattern, as long as they lie in the visible region. For $d = 0.25\lambda$, and in general for any $d < \lambda/2$, only a subset of these zeros will fall in the visible region. The zeros of the 8-element array patterns of Fig. 22.7.1 are shown in Fig. 22.7.2.

The two most important features of the uniform array are its 3-dB beamwidth $\Delta\psi_{3dB}$, or $\Delta\phi_{3dB}$ in angle-space, and its sidelobe level R. These parameters are shown in Fig. 22.7.3, for an 8-element uniform array with $d = 0.5\lambda$.
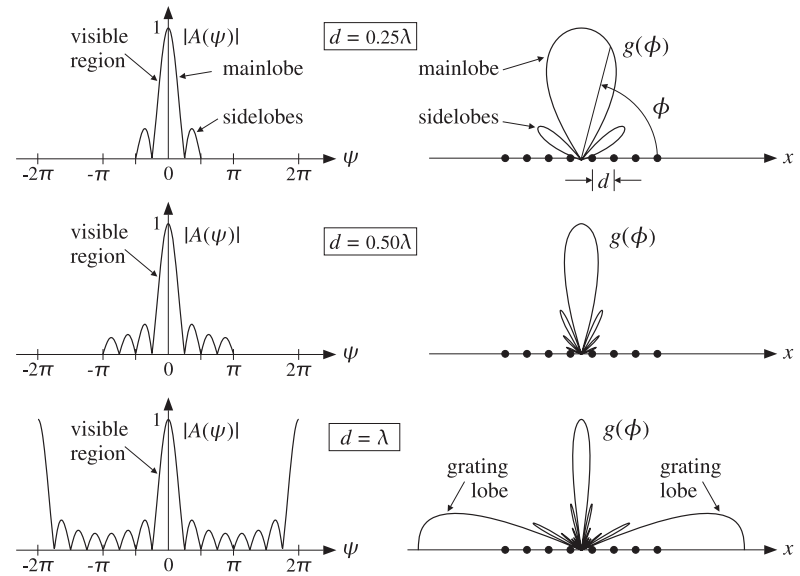
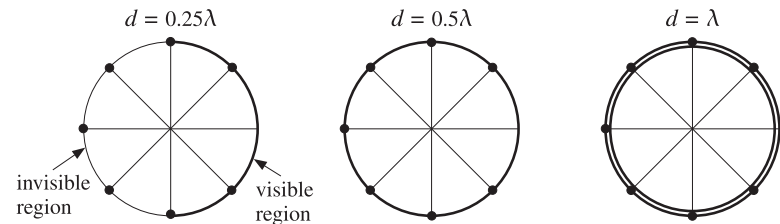**Fig. 22.7.1** Array factor and angular pattern of 8-element uniform array.

Fig. 22.7.2 Zero locations and visible regions of 8-element uniform array.

For N larger than about 5–6, the sidelobe level becomes independent of N and has the limiting value of $R = 13$ dB. Similarly, the beamwidth in ψ-space—defined as the full width of the mainlobe at the half-power level—takes the simple form:

$$\boxed{\Delta\psi_{3dB} = 0.886 \frac{2\pi}{N}} \qquad \text{(3-dB width in } \psi\text{-space)} \qquad (22.7.5)$$

The first nulls in the array factor about the mainlobe are at $\pm\psi_1 = \pm 2\pi/N$, and therefore, $2\pi/N$ represents half of the base of the mainlobe.

The 3-dB width $\Delta\phi_{3dB}$ in angle space can be obtained by differentiating the equation $\psi = kd\cos\phi$, that is, $d\psi = (\partial\psi/\partial\phi)d\phi = (-kd\sin\phi)d\phi$. Evaluating the derivative
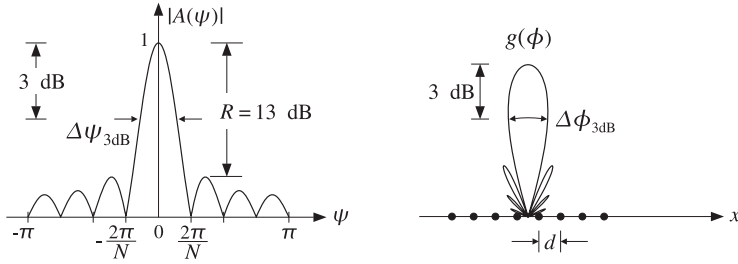
Fig. 22.7.3 Mainlobe width and sidelobe level of uniform array.

at broadside ($\phi = 90^\circ$) and assuming a narrow mainlobe, we have:

$$\Delta\psi_{3dB} = \left|\frac{\partial\psi}{\partial\phi}\right| \Delta\phi_{3dB} = kd\,\Delta\phi_{3dB}$$

Solving for $\Delta\phi_{3dB}$, we obtain $\Delta\phi_{3dB} = \Delta\psi_{3dB}/(kd) = 0.886\,(2\pi/N)/(2\pi d/\lambda)$, or

$$\boxed{\Delta\phi_{3dB} = 0.886\,\frac{\lambda}{Nd}} \qquad \text{(3-dB width at broadside)} \qquad (22.7.6)$$

The mainlobe beamwidth gets narrower with increasing N, while the relative sidelobe level remains the same. To achieve better (lower) sidelobe levels, one must use non-uniform weights obtained from non-rectangular windows.

The quantity $D = Nd$ is the effective *aperture* of the array. Thus, we recognize Eq. (22.7.6) as the classical *Rayleigh limit* on the resolving power of an optical system, which states that the *angular resolution* achieved by an aperture of length D is essentially λ/D.

The beamwidth expression (22.7.5) and the 13-dB sidelobe level can be justified as follows. The peak of the first sidelobe occurs approximately half-way between the first two nulls, that is, at $\psi = 3\pi/N$. More precisely, it occurs at $\psi = 2.8606\pi/N$. Thus, the sidelobe level in dB will be:

$$R = -20\log_{10}\left|\frac{A(\psi)}{A(0)}\right|_{\psi=2.8606\pi/N} = -20\log_{10}\left|\frac{\sin(1.4303\pi)}{N\sin(1.4303\pi/N)}\right|$$

$$\simeq -20\log_{10}\left|\frac{\sin(1.4303\pi)}{N(1.4303\pi/N)}\right| = -20\log_{10}\left|\frac{\sin(1.4303\pi)}{1.4303\pi}\right| = 13.26\text{ dB}$$

where we used the small-x approximation, $\sin x \simeq x$, in the denominator, which is justified when N is large. Setting $x = N\psi/2$, the sidelobe peak corresponds to the secondary maximum of the approximate array factor $\sin x/x$, which by differentiation leads to the equation $x = \tan x$, having solution $x = 1.4303\pi$, or $\psi = 2x/N = 2.8606\pi/N$.

The 3-dB width $\Delta\psi_{3dB}$ is twice the 3-dB or half-power frequency ψ_3, defined to be the solution of the equation:

$$|A(\psi_3)|^2 = \left|\frac{\sin(N\psi_3/2)}{N\sin(\psi_3/2)}\right|^2 = \frac{1}{2}$$

Because ψ_3 is always smaller than $2\pi/N$, it will be small for large N, and therefore, we may make the same approximation in the denominator as above, giving the simplified equation:

$$\left|\frac{\sin(N\psi_3/2)}{N\psi_3/2}\right|^2 = \left|\frac{\sin x_3}{x_3}\right|^2 = \frac{1}{2}$$

where $x_3 = N\psi_3/2$. The quantity x_3 is determined to be the constant $x_3 = 0.443\pi$. Thus, $\psi_3 = 2x_3/N = 0.443\,(2\pi/N)$, and $\Delta\psi_{3dB} = 2\psi_3 = 0.886\,(2\pi/N)$.

22.8 Array Directivity

The value of kd has an impact also on the directivity of an array. In the array processing literature, the directivity of an array is usually defined with reference to a z-directed array consisting of *isotropic* radiators. The wavenumber is $\psi = kd\cos\theta$ and the maximum of the array factor is assumed to occur at broadside $\theta = 90^\circ$, or $\psi = 0$. This basically means that the array factor will have a lowpass shape as a function of ψ, with a maximum value at dc given by

$$|A(0)| = \left|\sum_{n=0}^{N-1} a_n\right|$$

It follows that the normalized power gain of the array will be:

$$g(\theta) = c|A(\theta)|^2$$

where $c = 1/|A(0)|^2$. The corresponding beam solid angle will be:

$$\Delta\Omega = 2\pi\int_0^\pi g(\theta)\sin\theta\,d\theta = 2\pi\int_0^\pi c|A(\theta)|^2\sin\theta\,d\theta$$

Changing variables of integration from θ to ψ, which varies over the visible region (22.5.1), we obtain:

$$\Delta\Omega = \frac{2\pi}{kd}\int_{-kd}^{kd} c|A(\psi)|^2\,d\psi = \frac{2\pi c}{kd}\int_{-kd}^{kd}\sum_{n,m} a_n a_m^* e^{j(n-m)\psi}\,d\psi$$

Performing the integration, we get

$$\Delta\Omega = 4\pi c\sum_{n,m} a_n a_m^* \frac{\sin(kd(n-m))}{kd(n-m)}$$

Therefore, the directivity of the array becomes:

$$D = \frac{4\pi}{\Delta\Omega} = \frac{\left|\sum_n a_n\right|^2}{\sum_{n,m} a_n a_m^* \dfrac{\sin(kd(n-m))}{kd(n-m)}} \qquad (22.8.1)$$

In the particular case of half-wavelength spacing $d = \lambda/2$ or $kd = \pi$, the sinc function acts as a delta function $\delta(n - m)$, and the sum simplifies into:

$$D = \frac{|\sum_{n=0}^{N-1} a_n|^2}{\sum_{n=0}^{N-1} |a_n|^2} \tag{22.8.2}$$

The maximum of this quantity is reached when all the coefficients are equal to each other. The common value may be adjusted so that their sum is unity, that is:

$$a_n = \frac{1}{N}, \qquad n = 0, 1, \ldots, N - 1$$

The maximized value of D becomes:

$$D_{\max} = N \tag{22.8.3}$$

Thus, the uniform array with half-wavelength spacing achieves *maximum directivity* equal to the *number* of array elements. This result is analogous to finding the optimum N-tap lowpass FIR filter that minimizes the noise reduction ratio, that is, the sum of the squares of its coefficients.

For arbitrary spacing d, it is shown in Problem 22.6 that the optimum array vector $\mathbf{a} = [a_0, a_1, \ldots, a_{N-1}]^T$ that maximizes (22.8.1), and the corresponding maximum directivity, are given by:

$$\mathbf{a} = A^{-1}\mathbf{u}, \qquad D_{\max} = \mathbf{u}^T A^{-1}\mathbf{u} \tag{22.8.4}$$

where $\mathbf{u} = [1, 1, \ldots, 1]^T$ is a vector of N ones and A is the so-called *prolate matrix* [1274] with matrix elements:

$$A_{nm} = \frac{\sin(kd(n - m))}{kd(n - m)}, \quad 0 \leq n, m \leq N - 1 \tag{22.8.5}$$

The coefficients $\mathbf{a}$ may be renormalized such that their sum is unity. When d is an integer multiple of $\lambda/2$, the prolate matrix reduces to the $N \times N$ identity matrix, resulting into (22.8.3).

22.9 Array Steering

An array is typically designed to have maximum directive gain at broadside, that is, at $\phi = 90^o$ (for an array along the x-axis.) The maximum of the array factor $A(\psi)$ corresponds to $\psi = kd\cos\phi = 0$, so that $|A|_{\max} = |A(0)|$.

We wish to "electronically" rotate, or steer, the array pattern towards some other direction, say ϕ_0, without physically rotating it. The corresponding wavenumber at the desired look-direction will be:

$$\boxed{\psi_0 = kd\cos\phi_0} \qquad \text{(steering phase)} \tag{22.9.1}$$

Such steering operation can be achieved by *wavenumber translation* in ψ-space, that is, replacing the broadside pattern $A(\psi)$ by the translated pattern $A(\psi - \psi_0)$. Thus, we define:

$$\boxed{A'(\psi) = A(\psi - \psi_0)} \qquad \text{(steered array factor)} \tag{22.9.2}$$

and the translated wavenumber variable,

$$\boxed{\psi' = \psi - \psi_0 = kd(\cos\phi - \cos\phi_0)} \qquad \text{(steered wavenumber)} \tag{22.9.3}$$

Then, $A'(\psi) = A(\psi')$. The maximum of $A'(\psi)$ will coincide with the maximum of $A(\psi')$, which occurs at $\psi' = 0$, or equivalently at $\psi = \psi_0$, or at angle $\phi = \phi_0$. Fig. 22.9.1 illustrates this wavenumber translation process and the corresponding rotation of the angular pattern, for an 11-element uniform array with $d = \lambda/2$, steered from broadside to $\phi_0 = 60^o$. The MATLAB code for the last two graphs was:

```
d=0.5; N=11; ph0=60;
a = uniform(d, ph0, N);           % steered uniform weights
[g, phi] = gain1d(d, a, 400);     % calculate normalized gain g(φ)
psi = 2*pi*d*cos(phi);            % φ to ψ transformation
figure; plot(psi/pi, sqrt(g));    % plot in ψ space
figure; dbz(phi, g, 30, 20);      % azimuthal gain plot in dB
```
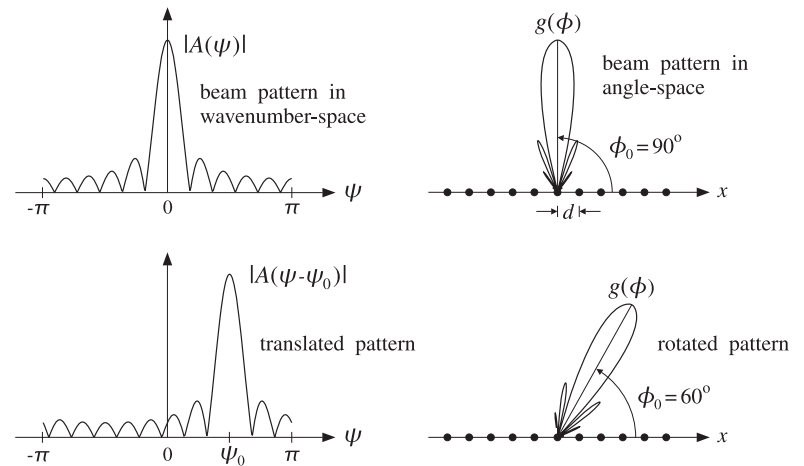

Fig. 22.9.1 Array steering or scanning by translation in wavenumber space.

It follows from the translation theorem of Fourier transforms that the weight coefficients a'_n of the translated pattern $A'(\psi)$ will be given by:

$$\boxed{a'_n = a_n e^{-j\psi_0 n}} \qquad \text{(steered array weights)} \tag{22.9.4}$$

so that we have:

$$A'(\psi) = \sum_n a'_n e^{j\psi n} = \sum_n a_n e^{j(\psi - \psi_0)n} = \sum_n a_n e^{j\psi' n} = A(\psi')$$

Because of the progressive phase factors $e^{-j\psi_0 n}$ in the weights a'_n, the steered or scanned array is sometimes called a *phased* or *scanning* array.

The time-domain version of array steering is AM modulation, in which a baseband signal is translated up in frequency by modulating with it a sinusoidal carrier, much like Eq. (22.9.4). Frequency translation is also used in DSP for mapping a lowpass filter into a bandpass one and for designing filter banks. We will use it in Sec. 23.4 to design arrays with angular sector patterns.

The MATLAB functions steer.m and scan.m of Appendix L can be used to implement Eq. (22.9.4). Their usage for even or odd number of array elements is discussed in Sec. 23.1.

Example 22.9.1: In Examples 22.3.1 and 22.3.2, we considered the three cases having progressive phases $\psi_0 = 0, \pi, \pi/2$. These may or may not correspond to a physical steering angle ϕ_0, depending on whether or not ψ_0 lies in the visible region.

In the case $\psi_0 = \pi$ and $d = 0.25\lambda$, we have $\psi = 0.5\pi \cos \phi$, and therefore it is not possible to find a solution for $0.5\pi \cos \phi_0 = \psi_0 = \pi$. However, the array factor does correspond to a pattern rotated towards endfire. This can be seen from the expression,

$$|A(\psi)| = |1 - e^{j\psi}| = 2\,|\sin(\psi/2)\,| = 2\,|\sin(0.25\pi \cos \phi)\,|$$

which is maximum towards endfire and minimum towards broadside. In the case $\psi_0 = \pi/2$ and $d = 0.25\lambda$, there is a solution to $0.5\pi \cos \phi_0 = \psi_0 = 0.5\pi$, that is, $\phi_0 = 0^o$, which corresponds to the maximum of the steered array.

In the case $\psi_0 = \pi$ and $d = 0.5\lambda$, we have $\psi = \pi \cos \phi$, and the solution to the equation $\pi \cos \phi_0 = \pi$ is $\phi_0 = 0^o$. However, because the phase $\psi_0 = \pi$ is indistinguishable from the phase $\psi_0 = -\pi$ (both lead to $e^{-j\psi_0} = -1$), we will also have the solution to $\pi \cos \phi_0 = -\pi$, which is $\phi_0 = 180^o$.

In the case $\psi_0 = \pi/2$ and $d = 0.5\lambda$, the solution to $\pi \cos \phi_0 = \pi/2$ is $\phi_0 = 60^o$, which corresponds to the maximum, as can be seen in Fig. 22.3.1.

In the case $\psi_0 = \pm\pi$ and $d = \lambda$, we have $\psi = 2\pi \cos \phi$, and the solutions to $2\pi \cos \phi_0 = \pm\pi$ are $\phi_0 = 60^o$ and 120°.

Finally, in the case $\psi_0 = \pi/2$ and $d = \lambda$, the solution to $2\pi \cos \phi_0 = \pi/2$ is $\phi^0 = 75.5^o$. However, there is another grating lobe maximum towards $\phi_0 = 138.6^o$, which corresponds to the solution of $2\pi \cos \phi_0 = -3\pi/2$. This is so because $\psi_0 = \pi/2$ and $\psi_0 = -3\pi/2$ are indistinguishable phases, both leading to $e^{-j\psi_0} = -j$.   □

The concepts of visible region, beamwidth, and the condition for absence of grating lobes, translate with minor modifications to the case of a steered array. As the angle ϕ varies over $0^o \le \phi \le 180^o$, the translated wavenumber ψ' of Eq. (22.9.3) varies over the shifted visible region:

$$\boxed{-kd\,(1 + \cos \phi_0) \le \psi' \le kd\,(1 - \cos \phi_0)} \qquad \text{(shifted visible region)} \qquad (22.9.5)$$

where its total width is again $2kd$. The condition for absence of grating lobes is obtained with the help of the inequality:

$$|\psi'| \le kd\,|\cos \phi - \cos \phi_0| \le kd\,(|\cos \phi| + |\cos \phi_0|) \le kd\,(1 + |\cos \phi_0|)$$

To ensure no grating lobes, ψ' must remain strictly less than 2π, which results in the sufficient condition: $kd\,(1 + |\cos \phi_0|) < 2\pi$, or replacing $kd = 2\pi d/\lambda$,

$$\boxed{d < \frac{\lambda}{1 + |\cos \phi_0|}} \qquad \text{(no grating lobes)} \qquad (22.9.6)$$

At broadside, $\phi_0 = 90^o$, this reduces to the earlier condition $d < \lambda$. At endfire, $\phi_0 = 0^o$ or 180°, it reduces to $d < \lambda/2$.

22.10 Array Beamwidth

Because the steered array has a mainlobe towards the direction ϕ_0, the beamwidth must be calculated by linearizing the map $\psi = kd \cos \phi$ about ϕ_0, that is,

$$\Delta\psi = \left|\frac{\partial \psi}{\partial \phi}\right|_{\phi_0} \Delta\phi = |-kd \sin \phi_0|\,\Delta\phi$$

which leads to the 3-dB beamwidth in angle-space:

$$\Delta\phi_{3dB} = \frac{1}{kd \sin \phi_0}\,\Delta\psi_{3dB}, \qquad \text{(3-dB width of steered array)} \qquad (22.10.1)$$

For window-based narrow-beam design methods, the beamwidth $\Delta\psi_{3dB}$ is approximately equal to the product of the beamwidth of the uniform array, Eq. (22.7.5), and a so-called *broadening factor* b, whose value depends on the choice of the window. Thus, we have:

$$\boxed{\Delta\psi_{3dB} = b\,\Delta\psi_{3\text{-dB, uniform}} = 0.886\,\frac{2\pi b}{N}} \qquad \text{(3-dB width in } \psi\text{-space)} \qquad (22.10.2)$$

Combining Eqs. (22.10.1) and (22.10.2) and replacing kd by $2\pi d/\lambda$, we get:

$$\Delta\phi_{3dB} = \frac{0.886}{\sin \phi_0}\,\frac{\lambda}{Nd}\,b, \qquad \text{(3-dB width in angle-space)} \qquad (22.10.3)$$

The 3-dB angles will be approximately $\phi_0 \pm \Delta\phi_{3dB}/2$. Because of the presence of $\sin \phi_0$ in the denominator, the beamwidth $\Delta\phi_{3dB}$ will broaden as the array is steered from broadside to endfire.

Exactly at endfire, $\phi_0 = 0^o$ or 180°, Eq. (22.10.3) fails and the beamwidth must be calculated by a different procedure. At $\phi_0 = 0^o$, the translated wavenumber $\psi' = \psi - \psi_0$ becomes $\psi' = kd\,(\cos \phi - 1)$. Using the approximation $\cos x = 1 - x^2/2$, we may relate the 3-dB angle ϕ_3 to the corresponding 3-dB wavenumber by:

$$\psi_3' = kd\,(\cos \phi_3 - 1) = kd\,((1 - \phi_3^2/2) - 1) = -\frac{1}{2}kd\phi_3^2$$

It follows that the 3-dB width in ψ-space will be $\Delta\psi_{3dB} = 2|\psi_3'| = kd\phi_3^2$. Solving for ϕ_3, we have $\phi_3 = \sqrt{\Delta\psi_{3dB}/kd}$. Thus, the 3-dB width in angle space will be $\Delta\phi_{3dB} = 2\phi_3$,

$$\Delta\phi_{3dB} = 2\sqrt{\frac{\Delta\psi_{3dB}}{kd}}, \qquad \text{(3-dB width at endfire)} \qquad (22.10.4)$$

The same expression also holds for endfire towards $\phi_0 = 180^\circ$. Replacing $\Delta\psi_{3dB}$ from Eq. (22.10.2), we find the width in angle space:

$$\Delta\phi_{3dB} = 2\sqrt{0.886\,\frac{\lambda}{Nd}\,b}\,, \qquad \text{(3-dB width in angle-space)} \qquad (22.10.5)$$

To summarize, the angular 3-dB width of the steered array can be computed in terms of the broadside 3-dB width in wavenumber space by:

$$\Delta\phi_{3dB} = \begin{cases} \dfrac{1}{kd\sin\phi_0}\,\Delta\psi_{3dB}\,, & \text{for } 0^\circ < \phi_0 < 180^\circ \\[3mm] 2\sqrt{\dfrac{\Delta\psi_{3dB}}{kd}}\,, & \text{for } \phi_0 = 0^\circ,\ 180^\circ \end{cases} \qquad (22.10.6)$$

In particular, if Eq. (22.10.2) is used:

$$\Delta\phi_{3dB} = \begin{cases} \dfrac{0.886}{\sin\phi_0}\dfrac{\lambda}{Nd}\,b\,, & \text{for } 0^\circ < \phi_0 < 180^\circ \\[3mm] 2\sqrt{0.886\,\dfrac{\lambda}{Nd}\,b}\,, & \text{for } \phi_0 = 0^\circ,\ 180^\circ \end{cases} \qquad (22.10.7)$$

In degrees, Eq. (22.10.7) reads as:

$$\Delta\phi_{3dB} = \begin{cases} \dfrac{50.76^\circ}{\sin\phi_0}\dfrac{\lambda}{Nd}\,b\,, & \text{for } 0^\circ < \phi_0 < 180^\circ \\[3mm] 107.86^\circ\sqrt{\dfrac{\lambda}{Nd}\,b}\,, & \text{for } \phi_0 = 0^\circ,\ 180^\circ \end{cases} \qquad (22.10.8)$$

In some designs such as binomial arrays, it is easier to determine $\Delta\psi_{3dB}$ directly from the array factor $A(\psi)$. In other designs, it is more convenient to estimate $\Delta\psi_{3dB}$ using Eq. (22.10.2).

The broadening factor b depends on the choice of the window and its sidelobe level. The larger the sidelobe attenuation, the larger the broadening factor. Some examples of broadening factors for different windows are given as follows:

Rectangular:	$b = 1,\quad (R = 13\ \text{dB})$
Hamming:	$b = 2,\quad (R = 40\ \text{dB})$
Taylor-Kaiser [1266]:	$b = \dfrac{6(R+12)}{155}$
Dolph-Chebyshev [1264]:	$b = 1 + 0.636\left[\dfrac{2}{R_a}\cosh\left(\sqrt{\text{acosh}^2(R_a)-\pi^2}\right)\right]^2$

where R and R_a represent the sidelobe level in dB and absolute units, respectively,

$$R = 20\log_{10}(R_a) \quad\Leftrightarrow\quad R_a = 10^{R/20} \qquad \text{(sidelobe level)} \qquad (22.10.9)$$

Here, R and R_a represent the *attenuation* of the sidelobe and, therefore, $R > 0$ and $R_a > 1$. The corresponding gain of the sidelobe relative to the mainlobe peak will be $R_a^{-1} = 10^{-R/20}$, which is less than one.

The MATLAB function bwidth.m of Appendix L implements Eq. (22.10.6). Its inputs are the quantities d, ϕ_0, $\Delta\psi_{3dB}$ and its output is the 3-dB width in degrees $\Delta\phi_{3dB}$. Its usage is:

```
Dphi = bwidth(d, phi0, Dpsi);      % map Δψ beamwidth to Δφ beamwidth
```

22.11 Problems

22.1 Show that the modified Friis formula (22.3.7) for two antennas over imperfect ground takes the following frequency-independent form in the limit of low grazing angles and $h_1 h_2 \ll \lambda r$:

$$\frac{P_2}{P_1} = G_1 G_2 \left(\frac{h_1 h_2}{r^2}\right)^2$$

22.2 Consider two horizontal dipoles I over imperfect ground, oriented along the x and y directions, as shown below. Show that the effect of the direct and ground-reflected rays can be obtained by considering an image dipole ρI.
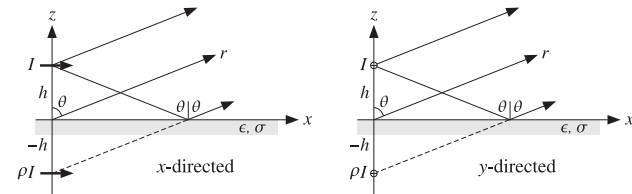

By considering the relative directions of the electric field along the direct and reflected rays, show that the resulting in array factor has the form:

$$A(\theta) = e^{jkh\cos\theta} + \rho\,e^{-jkh\cos\theta}$$

with $\rho = \rho_{TM}$ for the x-directed case and $\rho = \rho_{TE}$ for the y-directed one, where ρ_{TM}, ρ_{TE} are given by Eq. (7.4.4) with $n^2 = \epsilon_r - j60\sigma\lambda$.

22.3 A z-directed half-wave dipole is positioned in front of a 90° corner reflector at a distance d from the corner, as shown below. The reflecting conducting sheets can be removed and replaced by three image dipoles of alternating signs, as shown.
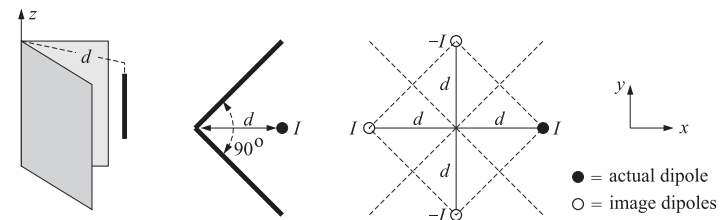
a. Thinking of the equivalent image problem as an array, determine an analytical expression for the array factor $A(\theta, \phi)$ as a function of the polar and azimuthal angles θ, ϕ.

b. For the values $d = 0.5\lambda$, $d = \lambda$, and $d = 1.5\lambda$, plot the azimuthal pattern $A(90^\circ, \phi)$ at polar angle $\theta = 90^\circ$ and for $-45^\circ \le \phi \le 45^\circ$.

c. For the cases $d = 0.5\lambda$ and $d = 1.5\lambda$, calculate the directivity D (in dB and in absolute units) and compare it with the directivity of a single half-wave dipole in the absence of the reflector.

d. Suppose that the corner reflector is flattened into a conducting sheet lying on the yz plane, i.e., the 90° angle between the sheets is replaced by a 180° angle. Repeat parts (a–c) in this case.

22.4 Four identical isotropic antennas are positioned on the xy-plane at the four corners of a square of sides a, as shown below. Determine the array factor $A(\phi)$ of this arrangement as a function of the azimuthal angle ϕ. (Assume the look direction is on the xy-plane.)
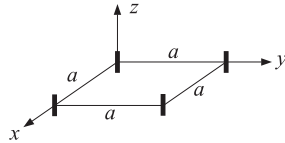
22.5 The array factor of a two-element array is given by:

$$g(\phi) = |a_0 + a_1 e^{j\psi}|^2 = \frac{1 + \sin\psi}{2}, \quad \psi = \frac{\pi}{2}\cos\phi$$

where ϕ is the azimuthal angle (assume $\theta = 90^\circ$) and ψ, the digital wavenumber. The array elements are along the x-axis at locations $x_0 = 0$ and $x_1 = d$.

a. What is the spacing d in units of λ? Determine the values of the array weights, $\mathbf{a} = [a_0, a_1]$, assuming that a_0 is real-valued and positive.

b. Determine the visible region and display it on the unit circle. Plot $|A(\psi)|^2$ versus ψ over the visible region. Based on this plot, make a rough sketch of the radiation pattern of the array (i.e., the polar plot of $g(\phi)$ versus $0 \le \phi \le 2\pi$).

c. Determine the exact 3-dB width of this array in angle space.

22.6 Defining the array vector $\mathbf{a}$ and the prolate matrix A via Eqs. (22.8.4) and (22.8.5), show that the directivity defined in Eq. (22.8.1) can be written in the compact form, where the dagger † indicates the conjugate transposed operation:

$$D = \frac{|\mathbf{u}^\dagger \mathbf{a}|^2}{\mathbf{a}^\dagger A \mathbf{a}} \tag{22.11.1}$$

a. Show that the maximum of D is attained for $\mathbf{a} = A^{-1}\mathbf{u}$ and that the maximized D is $D_{\max} = \mathbf{u}^\dagger A^{-1}\mathbf{u}$. Show that the value of $D_{\max}$ is not affected if $\mathbf{a}$ is defined with an arbitrary normalization factor μ, that is, $\mathbf{a} = \mu A^{-1}\mathbf{u}$.

b. Show that an equivalent problem is the minimization problem:

$$\mathbf{a}^\dagger A \mathbf{a} = \min, \quad \text{subject to} \quad \mathbf{u}^\dagger \mathbf{a} = 1$$

c. Show that (22.11.1) is a special case of the more general problem of the maximization of the *Rayleigh quotient*:

$$D = \frac{\mathbf{a}^\dagger Q \mathbf{a}}{\mathbf{a}^\dagger A \mathbf{a}} = \max$$

where A, Q are positive-definite Hermitian matrices. Show that the solution of this problem is the eigenvector corresponding to the maximum eigenvalue $\lambda = \lambda_{\max}$ of the generalized eigenvalue problem $Q\mathbf{a} = \lambda A \mathbf{a}$. Explain how this formulation leads to the same solution in the case of (22.11.1).

d. Show that the directivity (22.11.1) of a uniform array ($\mathbf{a} = \mathbf{u}$) is given by the two equivalent forms:

$$D_{\text{unif}} = \frac{|\mathbf{u}^\dagger \mathbf{u}|^2}{\mathbf{u}^\dagger A \mathbf{u}} = \frac{N^2}{N + 2\sum_{n=1}^{N-1}(N - |n|)\dfrac{\sin(kdn)}{kdn}}$$

22.7 *Computer Experiment—Optimum Directivity.* Using the matrix formulation of the previous problem, calculate the optimum directivity for an N-element array over the range of spacing values: $0.1 \le d/\lambda \le 2$ and plot it versus d. Carry this out for the values $N = 5, 10, 15$ and place the results on the same graph.

The directivity D of (22.11.1) can be evaluated for any given vector of array weights. Evaluate it for the uniform array $\mathbf{a} = \mathbf{u}$ and plot the results on the same graph as above. You should observe that directivity of the uniform array comes close to that of the optimum one for most (but not all) of the spacings d.

For each d and for the case $N = 15$, calculate the directivities of the array weights $\mathbf{a}$ designed with the MATLAB function `taylor1p` of the next chapter, with sidelobe attenuations of $R = 20$ $R = 30$ dB, and place them on the same graph.